Fabrication of conductive micro electrodes in diamond bulk using pulsed Bessel beams

Akhil Kuriakose [a,b], Andrea Chiappini [c], Belén Sotillo [d], Adam Britel [e], Pietro Aprà [e], Federico Picollo [e], Ottavia Jedrkiewicz [a,*]

[a] *Istituto di Fotonica e Nanotecnologie (IFN)-CNR, Udr di Como, Via Valleggio 11, 22100 Como, Italy*
[b] *Dipartimento di Scienza e Alta Tecnologia, Università dell'Insubria, Via Valleggio 11, 22100 Como, Italy*
[c] *Istituto di Fotonica e Nanotecnologie (IFN)-CNR, CSMFO and FBK Photonics Unit, Trento, Italy*
[d] *Department of Materials Physics, Faculty of Physics, Complutense University of Madrid, Plaza de Ciencias 1, 28040, Madrid, Spain*
[e] *Department of Physics and "NIS" Inter-departmental Centre, University of Torino National Institute of Nuclear Physics, sect. Torino, Via Pietro Giuria 1, 10125 Torino, Italy*

ABSTRACT

High-quality, in-bulk conductive graphitic microelectrodes are fabricated perpendicular to the surface of a 500 μm thick monocrystalline CVD diamond sample using pulsed Bessel beams. With a 12° cone angle beam, different pulse parameters are explored to optimize the graphitic wires which are written without sample translation. The quality of the electrodes and their electrical and structural properties have been analysed through current-voltage characterization and micro-Raman spectroscopy. We have found that higher pulse duration favours better conductivity while pulse energy has an optimum value for the same. This trend is confirmed by the presence and the different amounts of graphitic-like sp^2 bonded carbon revealed by the micro-Raman spectra in different configurations. Using suitable writing parameters, we are able to create electrodes with the resistivity of 0.04 Ω cm, which, to the best of our knowledge, is one of the lowest values ever reported in literature in the case of graphitic-like wires fabricated through laser micromachining.

1. Introduction

Diamond is an extraordinary crystal due to its remarkable properties such as hardness (Mohs index 10), scratch resistance, biocompatibility, chemical resistivity, high thermal conductivity and low thermal expansion coefficient [1,2]. The advancements in synthetic diamond manufacturing have brought down the cost of artificial diamonds such as the ones produced through chemical vapour deposition (CVD) or high-pressure high-temperature (HPHT) techniques thus resulting in mass production of the same. This has led to an increased utilization of them for various technological applications such as photonic and microfluidic platforms [3,4], radiation detection in particle physics [5], medical dosimetry [6] and high frequency electronics [7]. Recently, the presence of optically active defects such as the nitrogen-vacancy (NV) centres has made them a special attraction in quantum optics world due to their spin dependent fluorescence which can be used for optical spin readouts. In addition, NV centres find potential applications in

magnetometers due to Zeeman effect [4].

A common factor in almost all diamond–based devices is the presence of conductive graphitic microelectrodes (GMEs) which are primarily used for the application of electric fields or current transport/collection in various chips and detectors. Both surface and in-bulk electrodes are used but recently a 3-D, in-bulk orientation is widely researched due to their better performance and efficiency added with easy integration with other microstructures in diamond [8–10]. The two most prominent methods to create such electrodes in diamond are deep ion beam lithography (DIBL) and laser writing (LW). DIBL works on the fact that structural properties of the diamond undergo significant modification upon MeV ion micro-beam irradiation even creating graphitic-like structures by overcoming a critical defects density (graphite being another allotrope of carbon) both in single-crystal [11] and polycrystalline diamond [12]. In addition, ultrafast laser irradiation is also widely used for processing diamond crystals. A conventional Gaussian beam with moderately intense pulses can be used for the

optical break-down of the material thanks to the non-linear processes involved during the radiation-matter interaction, such as multiphoton absorption and avalanche ionization which are followed by the local transformation of diamond to graphitic-like carbon at the beam waist. As a result, a conducting graphitized region is formed in the insulator and a uniform translation of the laser focus throughout the crystal induces the formation of a wire-like graphitized region with a length of our choice [13].

Recently, non-conventional beams such as Bessel beams (BB) have been used for in-bulk micromachining of various materials [14]. In contrast to conventional Gaussian beams, finite energy Bessel beams have the advantage of a long focal length, the so-called Bessel zone, orders of magnitude larger than the typical Rayleigh range for a given spot size, thanks to its quasi-non-diffracting nature [15]. This means, it is possible to fabricate high aspect-ratio microstructures in different dielectrics without the need for sample translation. At the same time, due to their self-reconstruction property and their elongated focal zone, finite energy Bessel beams are ideal not only for internal micro structuring but also for high-impact technological applications such as high-speed cutting, welding or drilling of transparent materials [16–24].

There has been a lot of works related to laser writing of in-bulk GMEs in diamond, in particular related to the creation of electrodes parallel or orthogonal to the surface of the diamond. Fabrication of in-bulk electrodes which are perpendicular to the sample surface is always a challenge due to the cracking effect of diamond resulting from the crystal orientation which can end up with electrodes having unnecessary protrusions and collateral damage [25]. Moreover, the in-bulk micromachining using Gaussian beam needs aberration corrections, typically requiring adjustable lens systems, grating compressors [26], or a spatial light modulator (SLM) to avoid beam elongation and spreading at the focus [27]. Even though there has been a preliminary work of GME microfabrication using Bessel beams [28], a detailed study with different parameters and top-notch conductivity values is still absent. Here, in this work, we present the laser microfabrication of 3-D, in-bulk graphitic microelectrodes perpendicular to the sample surface by using Bessel beams without any sample translation, and we show that it is possible to fabricate, with suitable laser beam parameters and without the need of an SLM, GMEs presenting a compact and homogeneous central core despite the presence of lateral cracks that can be minimized. These are featured by good conductivity values, in line with or even higher than state-of- the-art values. Since the structural, geometrical and electrical properties of the graphitic-like carbon wires produced are strongly related to the laser processing parameters, a wide regime of pulse durations and energies are explored for the fabrication and characterization of GMEs.

2. Materials and methods

2.1. Experimental set-ups

The microfabrication studies were performed by means of a 20-Hz Ti: Sapphire amplified laser system (Amplitude) delivering 40-fs transform-limited pulses at 790 nm wavelength in the mJ pulse energy range. Since the laser compressor can be detuned to change the pulse duration, it is possible to work at both femtosecond and picosecond regimes. The experimental set-up at the micromachining table is shown in Fig. 1. The Bessel beam used in this research work is created by passing a spatially filtered Gaussian beam with a 5 mm beam through a fused silica axicon with 178° apex angle. A telescopic system formed by a 250 mm focal length lens (L_1) and a 0.45 N.A. 20× microscope objective (f_{obj} = 9 mm), leads to a final Bessel beam featured by 12° cone angle, a total central core size of about 3 μm and a total Bessel zone of 700 μm at the sample position. Note that the BB central core and, in the cases of highest energy pulses also few surrounding rings, are the only portions of the beam which will undergo nonlinear absorption and interact with the transparent material.

The transverse intensity beam profiling using a one lens imaging and a Charge-Coupled Device (CCD) camera (uEye) is carried out in air along the whole non-diffracting zone prior to micromachining [24]. The dichroic mirror placed between the lens and the objective deflects the beam and sends it orthogonally towards the sample placed on a micrometer precision 3D motorized stage (driven by SCA, system control application software, Altechna Rnd, Vilnius, Lithuania). A real-time observation of the sample surfaces during the micromachining process can be realized thanks to a backlighting Light Emitting Diode (LED) placed below the transparent sample and an imaging system using a lens (L) and another CCD (uEye). This allows a careful adjustment of the relative positioning of the BB focal length with respect to the sample thickness. In other words, by verifying that the top and bottom surface damage traces obtained in single shot are of similar shape and intensity, we can ensure for the case of in-bulk microfabrication that the central core peak intensity along the Bessel zone is symmetrically distributed across the sample, i.e., maximum intensity in the middle of the sample, and smaller intensity at the top and bottom. This prevents strong input interaction at the air/diamond interface where beam reshaping occurs because of the sudden change in the refractive index [29]. A detailed schematic of the whole experimental set up is given in [24].

The electrical characterization of the fabricated GMEs are performed through the current-voltage (IV) measurements. It involves a metallic deposition at one surface of the diamond covering only the particular electrode which is being tested and the opposite surface covered with
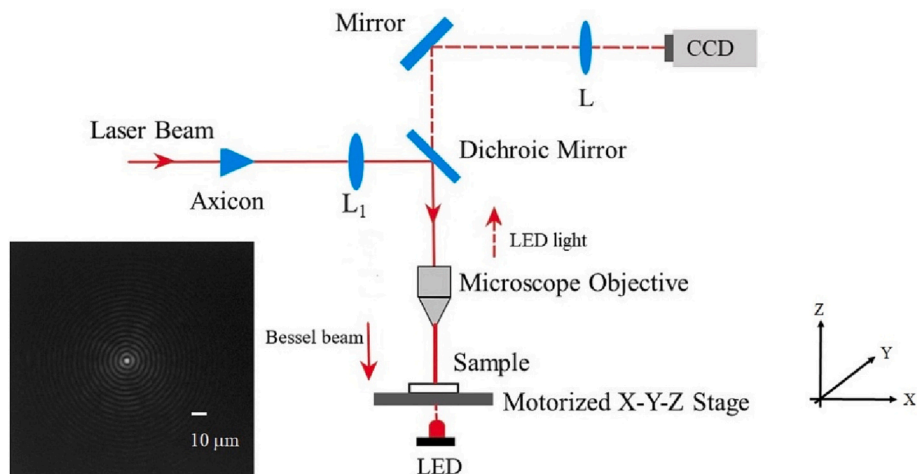

Fig. 1. Micromachining set-up scheme showing the orthogonal injection of the Bessel beam to the sample. On the bottom left, transverse profile of the BB recorded by a CCD camera.

silver paste such that the electrode acts as a closed circuit. A detailed description of the whole process is discussed in Section 2.3. The mask for the deposition is fabricated milling aluminium film (15 μm of thickness) with a nanosecond-pulsed Nd:YAG laser emitting in the IR (1064 nm), VIS (532 nm) or UV (355 nm). The pulse duration is 4 ns and the maximum energy per pulse is 0.6 mJ, resulting in an instantaneous power of 100 kW. The minimum beam spot size used was 5×5 μm^2 [30]. The PC-controlled system can manage both the sample displacement and the laser irradiation parameters (number of pulses, energy per pulse, wavelength) for each spot. Metal deposition for the fabrication of the electrodes was done using a thermal evaporator set-up consisting of a vacuum system which can lower the pressure to 10^{-5} mbar regime, a current source to heat up a crucible allowing the metal melting and evaporation and a SQM 160™ multifilm thickness monitor (INFICON) to measure the thickness of the deposition in real-time. The current-voltage characterization is therefore conducted with a 2-probe configuration in a custom probe station. It is possible to manually control the positioning of tungsten-carbide microprobes with micrometric spatial accuracy of different points of interest in the sample under analysis. The probes are connected to a high-precision Keithley™ 6487 voltage source, communicating with a computer through a LabVIEW system, which, in turn, measures the I-V curves. A "Leica Essential M50" optical microscope with an achromatic objective with magnification 0.63×, focal length of 148.2 mm and an eyepiece magnification of up to 100× interfaced with the I-V chamber allows for the accurate positioning of the microprobes on the sample. For annealing purposes, a ThermoConcept ROT 60/300/12 tubular oven was employed. The maximum achievable temperature with this system is 1200 °C, with a power of 3 kW. The control system allows the programming of treatment ramps according to the desired process protocol. Samples are loaded inside the tube in an inert alumina crucible. Annealing processes can be performed in vacuum (10^{-2} mbar) or with a continuous laminar flow of inert gas (Ar or N$_2$ supplied by gas cylinders) established inside the tube.

In order to highlight the effective transformation of diamond into graphitic-like carbon (featured by the presence of sp^2 hybridized carbon) in the laser-written microstructures, micro-Raman spectra are recorded using a Labram Aramis John Yvon Horiba system with a DPSS laser source at 532 nm. It is also equipped with a confocal microscope, an 1800 line mm^{-1} grating, and an air-cooled CCD camera. The Raman signal is collected in a backscattering configuration with a 100× objective, achieving a spatial resolution of about 1 μm.

2.2. Sample details

In this work, a monocrystalline type IIa CVD diamond with [100] orientation produced by MB Optics is used for the graphitic microelectrode fabrication. The dimensions of the sample are 3 mm × 3 mm with a thickness of 500 μm.

For the metal deposition as a part of current-voltage measurements, silver is used for the deposition of the superficial pads thus ensuring a good ohmic contact.

2.3. Experimental methods

The Bessel beam microfabrication of graphitic microelectrodes starts with the proper alignment of the sample such that it is perfectly flat together with the sample stage. This is crucial to make sure that the graphitic electrodes are perfectly perpendicular with respect to the top and bottom surfaces of the diamond sample. The micromachining is performed in a multiple pulse regime and the laser pulses are injected orthogonally to the sample surface (see Fig. 1); during the laser exposure, the graphitic microstructures start growing from the bottom surface (refer to Section 3.1 for the detailed description). The length of the generated wire depends on the number of pulses, controlled using an optical shutter [31]. It has been found that a minimum of 7000 Bessel pulses is enough to create an electrode of 500 μm length. Provided that

the Bessel zone covers the entire diamond thickness, with a laser repetition rate of 20 Hz, around 6 min are required for the fabrication of a single wire. Note that in the KHz regime, our technique would become one of the fastest in creating in-bulk microelectrodes of such length (as this would take just a few seconds for instance at 2 KHz repetition rate). All the GMEs reported in this work have been created utilizing 9000 pulses in order to work above the threshold number of pulses.

A schematic representation of the growth of a graphitic microelectrode is depicted in Fig. 2. It is worth mentioning that the conical nature of the BB and its lateral extent, featured by the surrounding rings carrying the conical energy reservoir, limit the minimum distance between two graphitic microstructures that can be fabricated without distortions but also the minimum distance from the diamond sample edge (in our case this was about 50 μm). After the fabrication of each electrode, the diamond sample is analysed under an optical microscope to make sure the in-bulk microstructure has reached the top surface with no breaks in between, so that the electrical characterization can be performed on the complete through-wires.

The current-voltage measurements require the presence of a conductive layer on both the top and bottom sides of the electrode. For this purpose, one side of the graphitic structure is deposited with a silver pad of 250×250 μm^2 area and the other is covered with silver paste. The shape of the metal pad is determined such that it is completely insulated from the other electrodes to avoid short circuits. Once the shape with appropriate dimensions is designed, the same structure is created in an aluminium foil by ablation using the Nd:YAG laser. The diamond sample is then aligned with the mask such that the metal will be deposited only on the surface of the target electrode and the rest of the diamond will be protected by the aluminium foil. The diamond is aligned in such a way that the metallic deposition happens on the bottom side since the top surface has got ablation marks because of the input air-diamond interface (where the ablation threshold is lower); filling up those (5 μm deep) craters would require a thicker metallic layer, which would drastically increase the time of deposition. Finally, a kapton polyimide tape is used to secure the diamond on the mask.

Once the alignment is done, the masked sample is mounted on the evaporator holder and the silver is deposited on the diamond. All the depositions have a thickness of 400 nm. After making sure the deposition position is accurate using an optical microscope, the metal deposited diamond is mounted on sample holder with silver paste. Once it is dried, the sample is set up in the IVT chamber for the current-voltage measurements. The two probes of the chamber are aligned on the sample such that one probe touches the deposited silver pad and the other one touches the silver paste. This completes the circuit and by
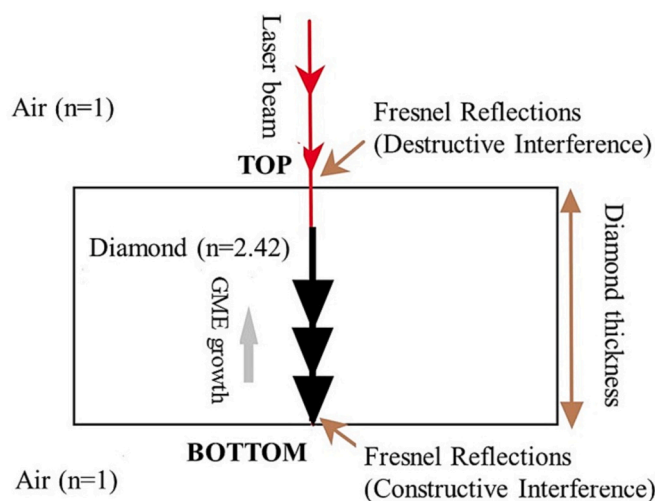

Fig. 2. Schematic representation of growth of a GME under Bessel beam irradiation.

setting up the parameters for the electrical measurements, the IV characteristics can then be collected. Fig. 3 represents the sample ready for the IV tests.

The electrical characterization of the GMEs has also been repeated after an annealing process, which is performed at 10^{-2} mbar pressure and 900 °C temperature for 1 h. All the measured resistivity values turned out to be generally lower after the annealing; for this reason in this work we shall present only the results obtained after the annealing of the diamond sample. A detailed study of the effect of annealing with a comparison of the electrical characteristics of the laser fabricated graphitic wires before and after the thermal treatment will be the object of future work.

3. Results and discussions

3.1. General graphitic microelectrode morphology

The phenomenon of graphitic wire formation occurs due to the primary optical breakdown of the diamond at a threshold fluence, which is followed by the formation of one or several discrete graphitized globules near the laser focus and this process continues as a propagation of a continuous graphitization wave from one of the globules towards the laser until the length of our choice [13]. Since graphite-like phases are good absorbers of radiation, the diamond layer adjacent to the first graphitic globule gets heated up, and this initiates a phase transition. In the case of a Gaussian beam, the focus is shifted and scanned throughout the bulk while the Bessel beam makes use of its long non-diffracting zone with multiple shots creating an electrode with the desired length. A lateral view of some GMEs written in a 500 μm thick diamond sample using a 12° cone angle pulsed Bessel beam with different pulse durations and energies, are shown for illustration in Fig. 4. Note that when using 10 ps pulses the graphitic wire formation occurs only for pulse energies above 5 μJ.

It is observed that when a high-power laser pulse passes through a transparent dielectric material, the threshold for optical damage of the exit surface is less than the threshold for damage of the entrance surface [29]. When a light pulse enters the material at a normal incidence, as shown in Fig. 2, there is a reflection at the air-dielectrics boundary (top). If the refractive index of the material is way greater than that of air (as in the case of diamond), the reflected light wave suffers a phase shift of 180° with respect to the incident light wave. This phase shift leads to destructive interference of the light resulting in a reduced electric field intensity. Meanwhile, the exit side (bottom) experiences the opposite. When this transmitted light pulse exits the sample, there is again a

reflected wave at the diamond-air interface, but this time the phase shift is zero since the wave is travelling from a high refractive index medium to a low refractive index medium and therefore, there is a constructive interference at the exit side. This leads to an increased field intensity, thus reducing the damage threshold of the transparent material at the bottom surface.

In Bessel beam microfabrication, where the elongated focal length of the beam crosses the whole sample thickness, the Fresnel reflections at each air/diamond interface seem to determine the direction of propagation of the graphitization wave. In this case because of the natural circular symmetry of the beam, the conical waves impinging at the exit interface and contributing to the core formation exactly on that plane will be back reflected and will overlap with the input conical waves. This will lead to a higher intensity of the beam in proximity of that interface similarly to the case of a focused Gaussian beam. In addition, here, the fact that the Bessel beam is featured by a focal length (Bessel zone) far larger than the sample thickness, implies that there will be conical waves contributing to the Bessel core reconstruction after the bottom surface, that will also be back reflected. These waves will be reflected towards the axis of the BB and thus will overlap with the conical waves responsible for the internal BB core formation, also leading to constructive interference (with lower intensity as we move towards the top surface). This could lead to a graphitic-like phase formation starting at the bottom and continuing in the direction of the laser until it reaches the top.

At high energies, the thickness of the electrode increases along with the cracking effect. While in the ps regime the graphitic microstructures are quite irregular in cross-section and exhibit cracks which become more and more evident as the pulse energy increases, the electrodes obtained in the fs regime are more regular in section and show traces of cracks only at high energy, namely above 8 μJ (see Fig. 4). More importantly, for very high intensities of the Bessel beam central core, the electrodes do not reach the top surface due to the nature of the Bessel beam. Indeed, the high damage at the top surface of the sample, with consequent graphitic-like phase formation at the air/diamond interface, blocks a portion of the Bessel beam which cannot penetrate just below the surface. Nevertheless, thanks to the conical energy reservoir [32] the beam gets again recreated after a small distance (few/tens μm length) from the top. This results in an in-bulk electrode length shorter than the sample thickness. Finally, we observed in our study, similarly to what shown in [31], that at low pulse durations such as 200 fs, a slightly larger number of pulses is required with respect to the normal threshold number for the graphitic wire to reach the top surface.

3.2. Role of pulse duration in GME fabrication

Since the aim of this work was to obtain the most uniform graphitic wires and the best conductivity values for the fabricated electrodes, we explored in the following the separate role of the pulse duration and of the pulse energy on the graphitic microstructures obtained by Bessel beam laser writing.

3.2.1. Morphology

We have observed that the morphology and thickness of the graphitic microstructures obtained at a given pulse energy remain almost invariant, irrespective of different pulse duration values. As an illustration, the evolution of GMEs fabricated with different pulse durations and for a 6 μJ pulse energy is presented in Fig. 5.

It can be observed that even though the size of the central core of the electrode remains the same (∼ 2.5 μm), the effect of cracking is more visible as the pulse duration is increased. In other words the lateral cracking giving rise to the feather-like structures becomes dominant with respect to the formation of a central homogeneous core of the microchannel in the ps regime, so that the compact and continuous nature of the central portion of the electrode is lost. The cracking effect at high pulse durations can be explained in terms of the stress change
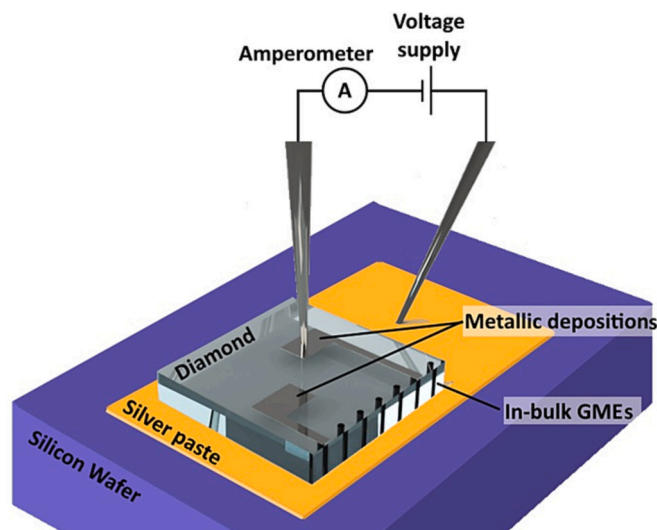

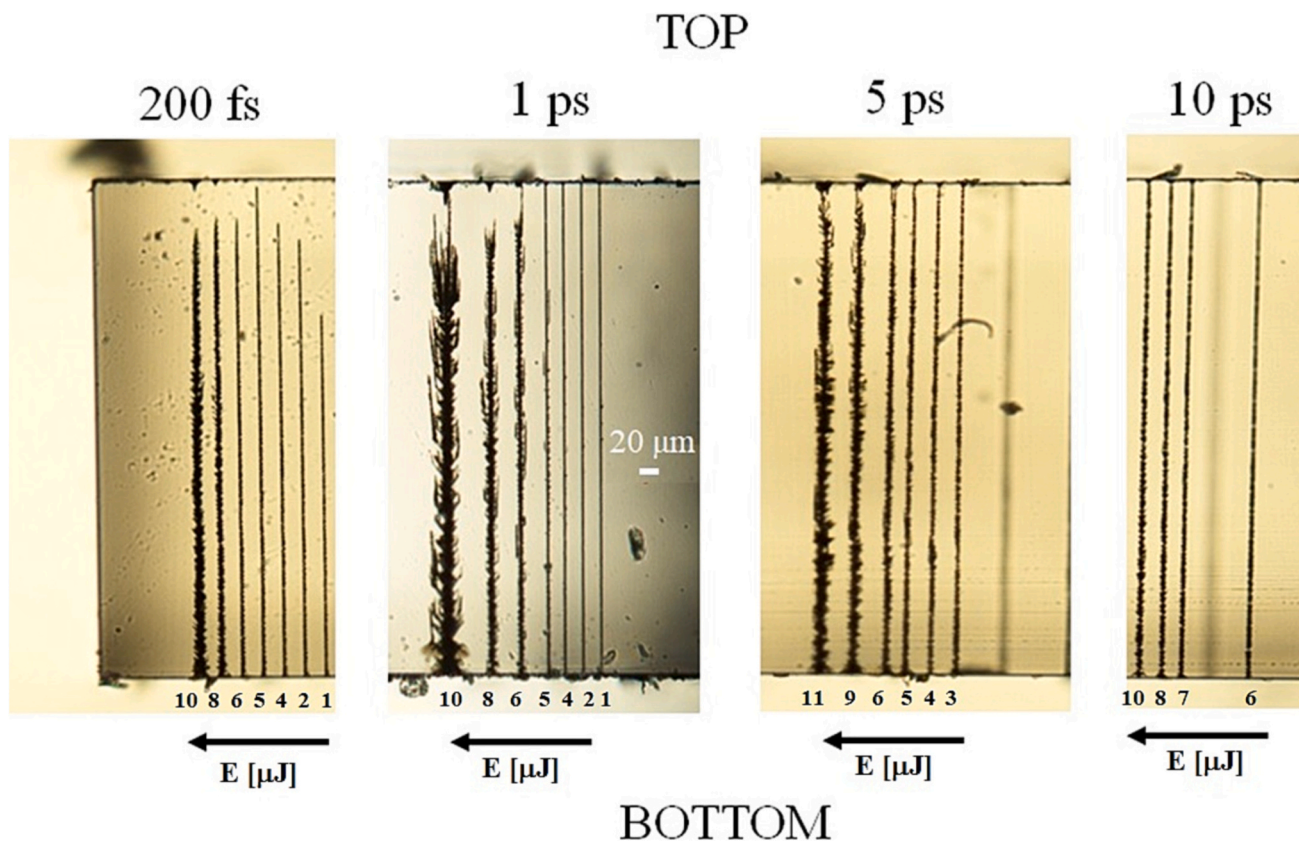**Fig. 3.** Schematic set-up for the electrical characterization of the in-bulk GMEs.

Fig. 4. Optical microscope images of the diamond sample (lateral view) showing the different GME structures obtainable with different beam parameters. The scale bar is the same for all images.
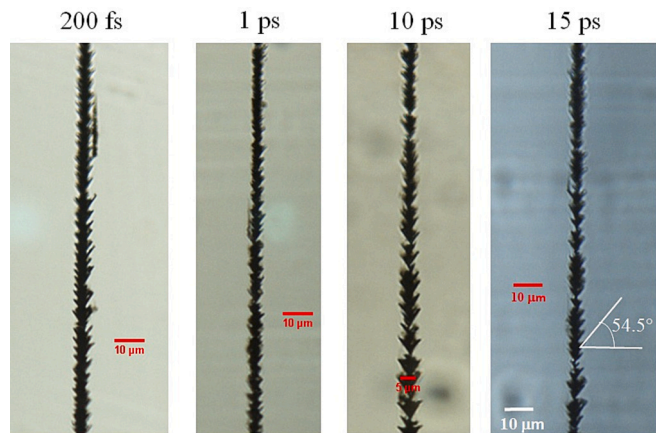

Fig. 5. Optical microscope images of a central portion of the diamond sample (lateral view) showing the variation of structural morphology of different GMEs with respect to pulse durations. The pulse energy used was 6.5 μJ. The magnification (featured by the scale bar clearly highlighted in white) is the same for all images.

and time taken for the graphitization process [33]. Diamond graphitization is a process that takes a few picoseconds [34]. When a part of the diamond lattice is converted to a graphitic-like phase under laser irradiation, its density becomes lower, resulting in a volume increase at that point and thus an internal strain formation [35]. If the laser pulse duration is shorter than a few picoseconds such as 200 fs in this case, when the pulse ends, a graphitic globule of minimal dimension (close to the laser spot size depending on the pulse energy) is formed without collateral damage in the near vicinity due to the "after-pulse" heating.

As the pulse duration is increased (i.e. 15 ps), even after the formation of the initial graphitic-like globule, a large amount of energy is still deposited (and thermal effects become dominant because of avalanche ionization) leading to the creation of highly strained areas where macroscopic cracks occur, since the local strain overcome the tensile strength of the diamond. This effect is even more pronounced at nanosecond pulse durations [33].

The directionality of the crack formation can be described based on the different cleavage energy/damage thresholds at different crystal orientations of the diamond lattice. As it is evident, the sharp protrusions emerging from the main graphitic lobe are at an angle with respect to the {001} surface. This angle is close to 54.5° which is exactly the angle between the {001} and {111} planes' orientations (Fig. 5). Interestingly, the {111} plane is the one with the lowest cleavage energy and strength in a diamond lattice [36]. This explains the repetitive and unidirectional growth of sharp microstructures as branches of the main graphitic lobe.

3.2.2. Current-voltage curves characteristics

We conducted a detailed study of the electrical properties of in-bulk wires perpendicular to the diamond sample written with different beam parameters. The resistance/resistivity of seventeen graphitic microelectrodes fabricated by varying the pulse energy between 3 and 8.5 μJ, with different pulse durations (200 fs, 1 ps, 10 ps and 15 ps) was measured with a current–voltage measurement set-up as detailed in Fig. 3. For all the tests mentioned in this work, we used a voltage range of −450 to 450 V, a compliance current of 25 mA, a step value of 5 V and a measurement time of 300 ms. The I-V tests for each electrode were conducted multiple times resulting in an error standard deviation of 5 %. In Fig. 6, we represent the I-V curves of various electrodes fabricated with a pulse energy of 6 μJ and with different pulse durations, namely 200 fs, 10 ps, and 15 ps respectively.
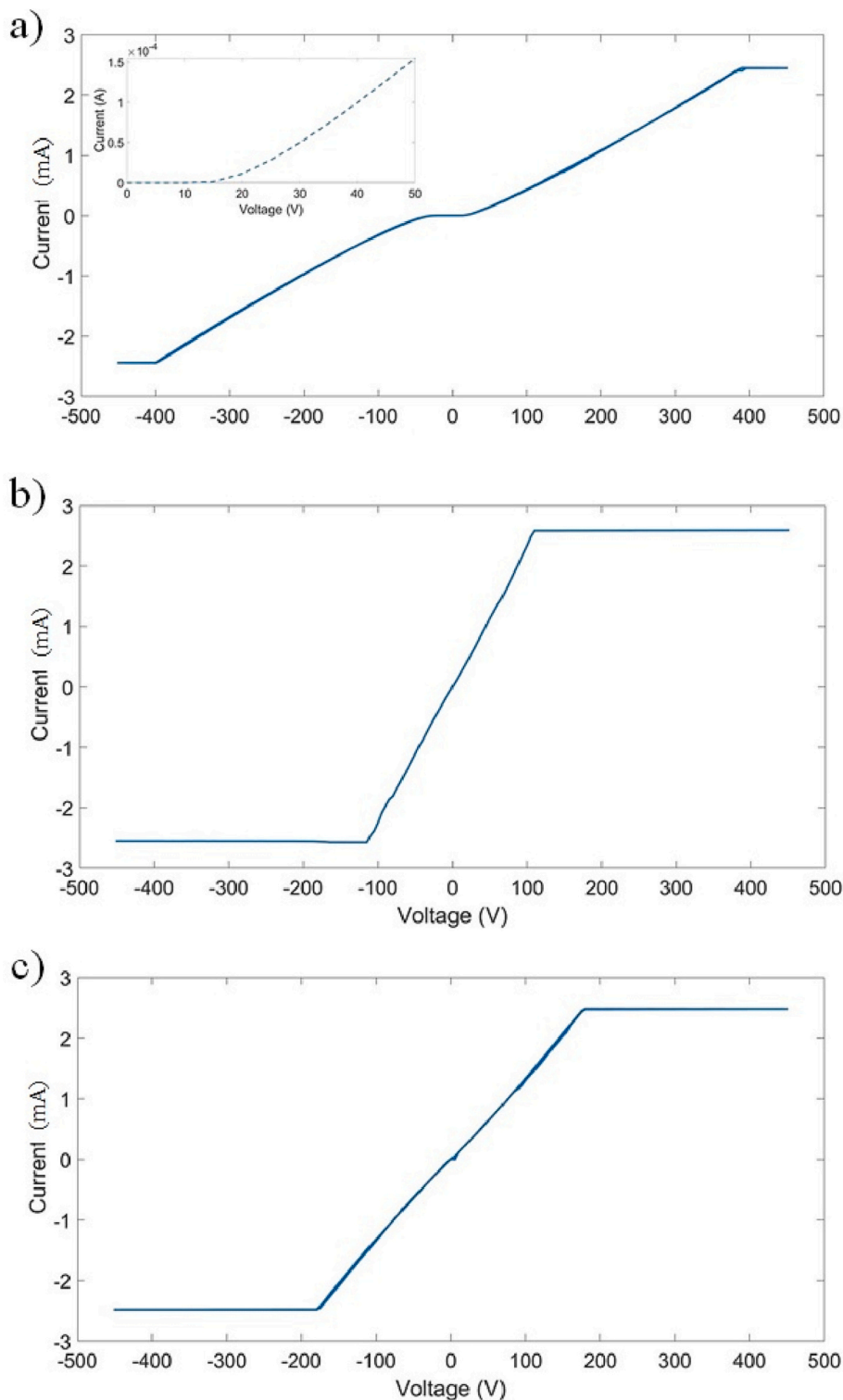
Fig. 6. Evolution of IV characteristics of three microelectrodes fabricated in diamond by Bessel beam machining with 200 fs pulses (a), 10 ps pulses (b) and with 15 ps pulses (c). In the first case we observe the presence of a 15 V potential barrier (see inset). Horizontal sections of the IV curves are due to the reaching of the current compliance.

The GMEs fabricated in different pulse duration regimes are characterized by different electrical behaviour. In particular, Fig. 6(a) shows the presence of a potential barrier of 15 V, only after which the electrode shows an ohmic behaviour. Note that the observation of a potential barrier has been already mentioned in previous work [37]. Even with a potential barrier, the electrode is featured by a resistivity value of 0.2 Ω cm which is top-notch with similar works such as [8,38,39]. The

resistivity values were calculated using the equation $\rho = RA/L$, where ρ is the resistivity, R is the resistance calculated from the graph, A is the cross-sectional area of the electrode (considering a diameter of about 2.5 μm) and L is the total length of the electrode (500 μm). The graphitic electrodes fabricated using lasers may not have continuous graphitic/conductive channels. Instead, there is a higher chance to have microscopic gaps between each graphitic globule and thus, to have a

continuous path for the charge flow, these gaps should be overcome. The voltage required to break down the gap is called the potential barrier/breakdown voltage. This theory has been confirmed by the findings of [40] where the presence of sp^2 carbon (associated with the conductive nature of the wire) was just 16 % by volume. Note that in [37,40] fs laser microfabrication was used, as in the case above described, thus substantiating the same behaviour as ours.

For graphitic microwires fabricated with higher pulse durations such as 10 ps and 15 ps, the behaviour of the corresponding IV curves is different. As shown in Fig. 6(b) and (c), the potential barrier is zero thus confirming a perfect ohmic behaviour of the electrodes. In addition, the resistivity of electrodes fabricated at 10 ps and 15 ps is reduced by more than 80 % and 60 % with respect to the electrode fabricated with 200 fs pulses, leading to an outstanding resistivity value of 0.04 and 0.07 Ω cm respectively. We attribute the slightly higher resistivity for the 15 ps case compared to the 10 ps case, to the fact that the electrode fabricated with the longer pulse duration is featured by a more discontinuous graphitic microstructure compared to that fabricated with 10 ps (see Fig. 5). As shown in Section 3.2.3, the lower resistivity values obtained for the ps regime are associated with a higher concentration of graphitic-like/sp^2 phase compared to the fs regime (see Fig. 7).

3.2.3. Micro-Raman analysis

In order to understand the crystalline structure of the laser-written graphitic electrodes created at different pulse durations, micro-Raman spectroscopy was performed by focusing the laser beam used for the measurement at the top of the wires (a few micrometer below the sample surface in order to maximize the signal). In Fig. 7 we present the spectra recorded in the central part of two wire cross-sections, corresponding to two different GMEs fabricated with 200 fs and 10 ps pulses respectively.

In both cases, the presence of the D-band (around 1351 cm^{-1}) and G-band (around 1585 cm^{-1}) together with the diamond peak (1332.2 cm^{-1}) suggests that the Bessel beam micromachining leads to a material conversion from sp^3 to sp^2 type bonding, thus transforming the diamond into a mixture of sp^2 carbon phases. In the case of fs laser fabrication, the intensity of the diamond peak remains high while the latter is almost suppressed in the ps regime. The opposite happens for the G and D bands, both common for sp^2 carbon systems (G-band arises from *vibrations in-plane of the sp^2 carbons*, whereas D-band is related to ring

breathing modes activated by defects or disorder). The G and D bands are dominant for electrodes created in the ps regime compared to those created in the fs regime. The ratio of the diamond peak and the G-band can also give a measure of the sp^2 carbon content inside the electrodes. This is, diamond peak is clearly visible in the fs regime, whereas it is almost covered by the sp^2 carbon signal in the ps regime. A higher content of sp^2-bonded carbon is thus revealed for the electrode fabricated with longer laser pulses, namely here 10 ps, in accordance with the results of our electrical measurements having highlighted in that case a greater electrode conductivity with respect to the fs case (given similar wires diameters), and as also reported in the literature [27].

However, a complete disappearance of the diamond phase may be discarded: although graphitic-like phases are more absorptive phases than diamond, a small diamond peak is still visible in the 10 ps Raman spectra. This observation agrees with the TEM results reported by Salter et al. [39]. Inside the wires, we have a mixture of damaged diamond and clusters of sp^2 carbon embedded within sp^3 phases. Finally, if we compare the shape and width of the D and G bands that appear in Fig. 7, both signals are similar. This is because the carbon phase formed has similar structural characteristics. Therefore, the increase in the conductivity is related to the increase of diamond transformation into graphitic-like clusters in the ps regime. Similar behaviour has been observed for example in carbon black materials, where an increase in the contact between the carbon particles produces an increase in the conductivity [41].

We could thus speculate that for the electrode fabricated with 10 ps laser pulse duration, larger size of the graphitic-like globules are formed during the radiation matter-interaction and possibly absence of micro-gaps between them may contribute to a smooth flow of charge and thus to the absence of the potential barrier as shown in Fig. 6(b). A detailed study of the variation of the potential barrier with respect to different laser writing parameters will be the object of a future work.

As we have pointed out before, the material that we have inside the wires is a mixture of damaged diamond and sp^2 bonded clusters. This is seen in the Raman signal by an increase of the G and D bands, along with an increase in the recorded background (due to the damaged material). If we remove the background and plot the value of the signal recorded at 1585 cm^{-1} (G-band), at 1360 cm^{-1} (D-band), we can see that these bands are confined inside the formed wires.

We observe that the highest intensity region for the modified material (highest D and G bands signal) has an extension of a few microns, which is in the same order of magnitude as the diameter of the Bessel written electrode. Given the good results of conductivity, it seems that the presence of lateral cracking in some wires do not have a negative impact on the electrical properties. This suggests that mainly the central core of the wire (the yellow-red region in the maps of Fig. 8), featured by the highest concentration of sp^2 graphitic-like phase, contributes to the charge flow and thus to the current.

3.3. Role of energy in GME fabrication

The dimensions of the laser written electrodes in diamond depend on the pulse energy. More precisely, it has been shown that the use of higher energy pulses leads to the fabrication of bigger electrodes [8]. Here, on one hand, we present some results from Bessel beam micromachining with a laser pulse duration of 10 ps and different pulse energy values. On the other hand, we compare the morphology of the graphitic wires obtained at fixed peak power by varying the energy and pulse duration values.

3.3.1. Morphology

In the case of Bessel-written GMEs, we have observed that a moderate increase in energy does not make a huge difference in the diameter of the electrode. Instead, a change in the crack length is observable (see Fig. 9). A noticeable variation in the electrode dimension occurs only at high energies. In Fig. 10 we analyse the effect of pulse energy on the
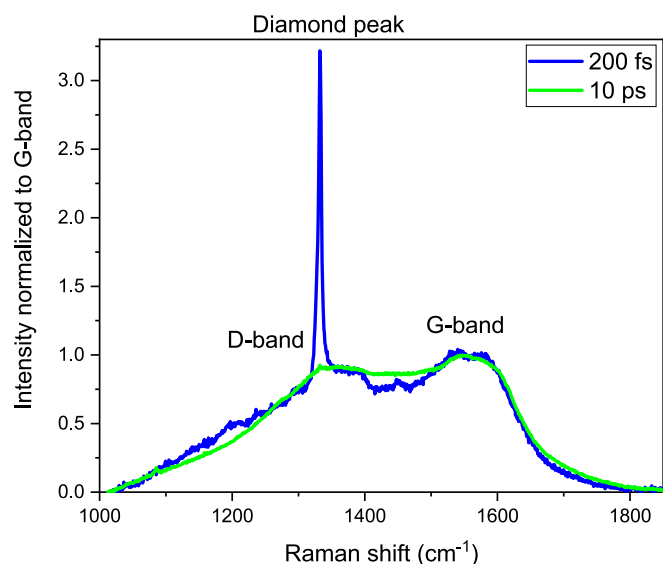

Fig. 7. Micro-Raman spectra recorded at the top of two electrodes fabricated respectively with 200 fs and with 10 ps pulses. The signal is normalized to the G-band.
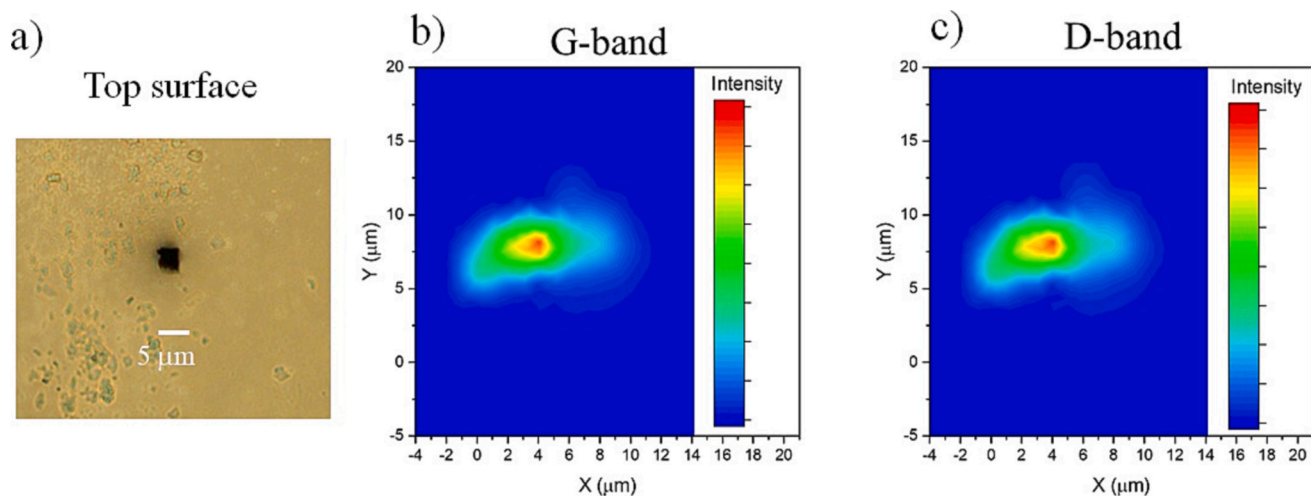
Fig. 8. (a) Optical microscope image of the top trace of a single GME fabricated with 10 ps pulses. (b) and (c) Contour plot of the same GME –indicating the evolution of G-band and D-band signals with respect to the scan position.
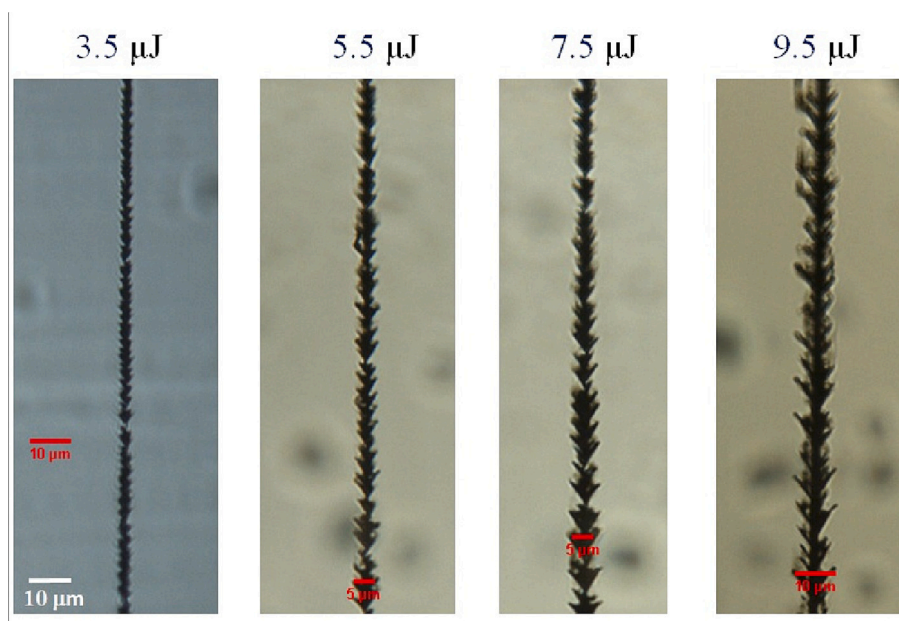

Fig. 9. Optical microscope images of a central portion of the diamond sample (lateral view) showing the different morphologies of GMEs obtained with different pulse energies (as indicated at the top of the images) and a pulse duration of 10 ps. The magnification (featured by the scale bar clearly highlighted in white) is the same for all images.
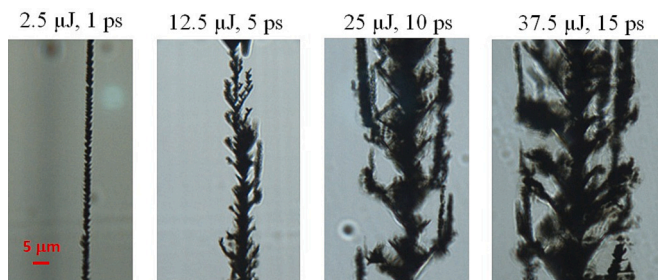

Fig. 10. Optical microscope images of a central portion of the diamond sample (lateral view) showing the different morphologies of GMEs obtained with different pulse energies and pulse durations (as indicated at the top of the images) in order to keep a fixed pump peak power (2.5×10^5 W). The scale bar is the same for all images.

graphitic wire morphology by keeping the peak power fixed, namely 250 kW.

Since the electrode diameter does not depend on the pulse duration (see Section 3.2.1), we may assume that pulse energy is the key parameter determining the electrode transverse size. At high energies, both the crack length and the dimensions of the main core of the microstructure increases.

3.3.2. Current-voltage curve characteristics

We have noticed that the I-V characteristics of the graphitic microelectrodes depend on the pulse energy used to write them. Higher energy leads to electrodes with huge dimensions and thus, less resistivity. Working at different energy values, we observed that the conductivity increases to a certain optimum value, and then it decreases. An example of such a trend for a 10 ps pulse duration fabrication regime is illustrated in Table 1, where we have reported the cases of four electrodes obtained

Table 1

Measured resistance and the corresponding resistivity of the graphitic wires fabricated in diamond by Bessel beam machining with 10 ps pulse duration and four different values of the pulse energy. The standard deviation error associated with the measurement is on the order of 5 %.

Energy (μJ)	Resistance (kΩ)	Resistivity (Ω cm)
3	82	0.08
6	41	0.04
7	72	0.07
8.5	81	0.08

with different Bessel beam pulse energies. The GME with the least resistivity value (0.04 Ω cm) is the one associated with the IV and microRaman results presented respectively in Fig. 6b and Fig. 7b. We believe that higher pulse energies might reduce the overall homogeneity and thus the quality of the electrode, therefore increasing its resistivity.

In general, by using the best laser parameters, we are able to fabricate electrodes with low resistivity values; in particular, for the electrode having resistivity of $\simeq 0.04$ Ω cm, this corresponds to an outstanding conductivity of 2500 S m^{-1}, which is, to the best of our knowledge, one of the best values compared to the literature, where resistivities of 0.1 Ω cm [42], 0.8 Ω cm [6], 0.06 and 0.9 Ω cm [38], 0.02 Ω cm [9], 1.6 Ω cm [43] and 3.9 Ω cm [8] at fs/ps fabrication regimes have been reported.

4. Conclusions

To summarize, in this work, we have shown that graphitic micro-electrodes (GMEs) can be fabricated in a monocrystalline CVD diamond sample using pulsed Bessel beams featured by a 3 μm diameter core and a non-diffracting zone of 700 μm (along beam direction) at 20 Hz repetition rate. The in-bulk fabrication of such electrodes perpendicular to the sample surface is possible in multiple shots with no sample translation along the beam propagation direction. Optimization of GMEs has been done using different laser writing parameters. In contrast to previous works reported in the literature, the optimization has been done without the use of techniques for aberration corrections (such as the use of a spatial light modulator) thanks to the already elongated focus of the Bessel beam and the longitudinal writing configuration. The morphological, electrical, and structural features of the electrodes have been analysed by optical microscopy, current-voltage tests and micro-Raman measurements, respectively. The results presented in this work refer to the micro-machined sample analysed after a thermal annealing.

Pulse duration plays a huge role in the conductivity of such in-bulk electrodes also for Bessel beam machining. We have confirmed that a higher pulse duration favours better conductivity. The micro-Raman spectra with highly intense diamond peak for electrodes fabricated in the fs regime compared to those fabricated in the ps regime confirm the same by denoting the better transformation of diamond into graphite at latter regime. We have shown that even though the transverse dimensions of the electrodes are not really affected by the pulse duration, for a given pulse energy, the length of the cracks increases slightly with increasing pulse duration. The dimensions of the electrode generally depend on the pulse energy. Even though there is no evident dimensional variation at low energy regimes, the morphological change is highly pronounced at high energies where the cracking effect is also highly dominant. For what concerns the conductivity of the GMEs, we found that it initially increases as the pulse energy increases, and this trend continues only until the optimum value of 0.04 Ω cm for 6 μJ is reached, after which the conductivity starts to decrease again.

Through the Bessel beam writing, it is possible to create graphitic microelectrodes with resistance as low as 41 kΩ opposed to the measured resistance of diamond which is close to 11 GΩ. We have measured for the best quality electrode a resistivity of 0.04 Ω cm, which, to the best of our knowledge, is one of the lowest values compared to the literature results and the lowest using Bessel beams. In addition, it is worth mentioning that it is the lowest value achieved for an in-bulk graphitic micro-electrode written perpendicular to the surface of the sample using laser micromachining. The relevance of this work lies in the optimization of the electrodes in terms of morphology (uniformity of the wires) and conductivity values, as GMEs are important for their integration with other microstructures such as optical waveguides, microfluidic channels, and optically active colour centres. This will be beneficial not only for the fabrication of photonic and microfluidic chips where graphitic electrodes can be incorporated for electric field generation and sensing, but also for a faster fabrication of electrode arrays for applications such as highly energetic radiation detectors in nuclear physics and medical dosimetry.

CRediT authorship contribution statement

O. J conceived and supervised the micromachining experiments, revised the entire manuscript. A. K realized the micromachining of the diamond sample, analysed the results, and wrote the first manuscript draft. Raman measurements were performed and analysed by A. C and B. S. The electrical measurements were performed by A. K with the help of A. B and P. An under the supervision of F. P. All authors revised the manuscript.

Declaration of competing interest

The authors declare that they have no known competing financial interests or personal relationships that could have appeared to influence the work reported in this paper.

Data availability

Data will be made available on request.

References

[1] Handbook of Industrial Diamonds and Diamond Films, Marcel Dekker, New York, 1998.

[2] R.J. Tapper, Diamond detectors in particle physics, Rep. Prog. Phys. 63 (8) (2000) 1273–1316, https://doi.org/10.1088/0034-4885/63/8/203.

[3] B. Sotillo, V. Bharadwaj, J.P. Hadden, M. Sakakura, A. Chiappini, T.T. Fernandez, S. Longhi, O. Jedrkiewicz, Y. Shimotsuma, L. Criante, R. Osellame, G. Galzerano, M. Ferrari, K. Miura, R. Ramponi, P.E. Barclay, S.M. Michael Eaton, Diamond photonics platform enabled by femtosecond laser writing, Sci. Rep. 6 (2016) 35566, https://doi.org/10.1038/srep35566.

[4] V. Bharadwaj, O. Jedrkiewicz, J.P. Hadden, B. Sotillo, M.R. Vázquez, P. Dentella, T. T. Fernandez, A. Chiappini, A.N. Giakoumaki, T.L. Phu, M. Bollani, M. Ferrari, R. Ramponi, P.E. Barclay, S.M. Eaton, Femtosecond laser written photonic and microfluidic circuits in diamond, JPhys photonics 1 (2019), 022001, https://doi.org/10.1088/2515-7647/ab0c4e.

[5] C. Bloomer, M.E. Newton, G. Rehm, P.S. Salter, A single-crystal diamond X-ray pixel detector with embedded graphitic electrodes, J. Synchrotron Radiat. 27 (3) (2020) 599–607, https://doi.org/10.1107/S160057752000140X.

[6] K. Kanxheri, L. Servoli, A. Oh, F. Munoz Sanchez, G.T. Forcolin, S.A. Murphy, A. Aitkenhead, C.J. Moore, A. Morozzi, D. Passeri, M. Bellini, C. Corsi, S. Lagomarsino, S. Sciortino, Evaluation of a 3D diamond detector for medical radiation dosimetry, J. Instrum. 12 (2017) 1, https://doi.org/10.1088/1748-0221/12/01/P01003.

[7] S.A.O. Russell, S. Sharabi, A. Tallaire, D.A.J. Moran, Hydrogen-terminated diamond field-effect transistors with cutoff frequency of 53 GHz, IEEE Electron Device Lett. 33 (2012) 1471–1473, https://doi.org/10.1109/LED.2012.2210020.

[8] T.V. Kononenko, V.I. Konov, S.M. Pimenov, N.M. Rossukanyi, A.I. Rukovishnikov, V. Romano, Three-dimensional laser writing in diamond bulk, Diam. Relat. Mater. 20 (2011) 264–268, https://doi.org/10.1016/j.diamond.2010.12.013.

[9] B. Sun, P.S. Salter, M.J. Booth, High conductivity microwires in diamond following arbitrary paths, Appl. Phys. Lett. 105 (2014), 231105, https://doi.org/10.1063/1.4902998.

[10] D. Tokunaga, M. Sato, S. Itoh, H. Hidai, T. Omatsu, S. Matsusaka, Focus movement distance per pulse dependence of electrical conductivity and diameter of diamond internal modification by picosecond laser, Sci. Rep. 12 (2022) 17371, https://doi.org/10.1038/s41598-022-21432-9.

[11] F. Picollo, A. Battiato, E. Carbone, L. Croin, E. Enrico, J. Forneris, S. Gosso, P. Olivero, A. Pasquarelli, V. Carabelli, Development and characterization of a diamond-insulated graphitic multi electrode array realized with ion beam lithography, Sensors 15 (2015) 515–528, https://doi.org/10.3390/s150100515.

[12] G. Tomagra, P. Aprà, A. Battiato, C.C. Ruvolo, A. Pasquarelli, A. Marcantoni, E. Carbone, V. Carabelli, P. Olivero, F. Picollo, Micro graphite-patterned diamond sensors: towards the simultaneous in vitro detection of molecular release and action potentials generation from excitable cells, Carbon 152 (2019) 424–433, https://doi.org/10.1016/j.carbon.2019.06.035.

[13] K.K. Ashikkalieva, Laser-induced graphitization of diamond bulk: the state of the art (a review), Phys. Wave Phenom. 30 (2022) 1–16, https://doi.org/10.3103/S1541308X22010034.

[14] M. Duocastella, C.B. Arnold, Bessel and annular beams for materials processing, Laser Photonics Rev. 6 (2012) 607–621, https://doi.org/10.1002/lpor.201100031.

[15] J. Durnin, J.J. Miceli, J.H. Eberly, Comparison of Bessel and Gaussian beams, Opt. Lett. 13 (1988) 79–80, https://doi.org/10.1364/ol.13.000079.

[16] M.K. Bhuyan, P.K. Velpula, J.P. Colombier, T. Olivier, N. Faure, R. Stoian, Single-shot high aspect ratio bulk nanostructuring of fused silica using chirp-controlled ultrafast laser Bessel beams, Appl. Phys. Lett. 104 (2014), 021107, https://doi.org/10.1063/1.4861899.

[17] M.K. Bhuyan, O. Jedrkiewicz, V. Sabonis, M. Mikutis, S. Recchia, A. Aprea, M. Bollani, P. Di Trapani, High-speed laser-assisted cutting of strong transparent materials using picosecond Bessel beams, Appl. Phys. 120 (2015) 443–446, https://doi.org/10.1007/s00339-015-9289-7.

[18] R. Meyer, M. Jacquot, R. Giust, J. Safioui, L. Rapp, L. Furfaro, P.-A. Lacourt, J. M. Dudley, F. Courvoisier, Single-shot ultrafast laser processing of high-aspect-ratio nanochannels using elliptical Bessel beams, Opt. Lett. 42 (2017) 4307–4310, https://doi.org/10.1364/OL.42.004307.

[19] R. Stoian, M.K. Bhuyan, G. Zhang, G. Cheng, R. Meyer, F. Courvoisier, Ultrafast Bessel beams: advanced tools for laser materials processing, Adv. Opt. Technol. 7 (2018) 165–174, https://doi.org/10.1515/aot-2018-0009.

[20] O. Jedrkiewicz, D. Valetti, P. Di Trapani, Etching and drilling of through-holes in thin glass by means of picosecond Bessel beams, SN Appl. Sci. 1 (2019) 1267, https://doi.org/10.1007/s42452-019-1328-0.

[21] J. Dudutis, R. Stonys, G. Račiukaitis, P. Gečys, Glass dicing with elliptical Bessel beam, Opt. Laser Technol. 111 (2019) 331–337, https://doi.org/10.1016/j.optlastec.2018.10.007.

[22] V.V. Belloni, V. Sabonis, P. Di Trapani, O. Jedrkiewicz, Burst mode versus single-pulse machining for Bessel beam micro-drilling of thin glass: study and comparison, SN Appl. Sci. 2 (2020) 1589, https://doi.org/10.1007/s42452-020-03327-4.

[23] V.V. Belloni, M. Bollani, S.M. Eaton, P. Di Trapani, O. Jedrkiewicz, Micro-hole generation by high-energy pulsed Bessel beams in different transparent materials, Micromachines 12 (2021) 455, https://doi.org/10.3390/mi12040455.

[24] A. Kuriakose, M. Bollani, P. Di Trapani, O. Jedrkiewicz, Study of through-hole micro-drilling in sapphire by means of pulsed Bessel beams, Micromachines 13 (4) (2022) 624, https://doi.org/10.3390/mi13040624.

[25] S.M. Pimenov, I.I. Vlasov, A.A. Khomich, B. Neuenschwander, M. Muralt, V. Romano, Picosecond-laser-induced structural modifications in the bulk of single-crystal diamond, Appl. Phys. 105 (2011) 673–677, https://doi.org/10.1007/s00339-011-6645-0.

[26] P. Wang, W. Chu, W. Li, Y. Tan, J. Qi, Y. Liao, Z. Wang, Y. Cheng, Aberration-insensitive three-dimensional micromachining in glass with spatiotemporally shaped femtosecond laser pulses, Opt. Lett. 43 (2018) 3485–3488, https://doi.org/10.1364/OL.43.003485.

[27] S.A. Murphy, M. Booth, L. Li, A. Oh, P. Salter, B. Sun, D. Whitehead, A. Zadoroshnyj, Laser processing in 3D diamond detectors, Nucl. Instrum. Methods. Phys. Res. A 845 (2017) 136–138, https://doi.org/10.1016/j.nima.2016.04.052.

[28] B.K. Canfield, L.M. Davis, Evaluation of Bessel beam machining for scalable fabrication of conductive channels through diamond, in: Proceedings of the SPIE 10092, Laser based Micro and Nanoprocessing XI, 100921U, 2017, https://doi.org/10.1117/12.2252615.

[29] M.D. Crisp, N.L. Boling, G. Dubé, Importance of Fresnel reflections in laser surface damage of transparent dielectrics, Appl. Phys. Lett. 21 (1972) 364–366, https://doi.org/10.1063/1.1654414.

[30] F. Picollo, S. Rubanov, C. Tomba, A. Battiato, E. Enrico, A. Perrat-Mabilon, C. Peaucelle, T.N. Tran Thi, L. Boarino, E. Gheeraert, P. Olivero, Effects of high-power laser irradiation on sub-superficial graphitic layers in single-crystal diamond, Acta Mater. 103 (2016) 665–671, https://doi.org/10.1016/j.actamat.2015.10.046.

[31] S. Kumar, B. Sotillo, A. Chiappini, R. Ramponi, P. Di Trapani, S.M. Eaton, O. Jedrkiewicz, Study of graphitic microstructure formation in diamond bulk by pulsed Bessel beam laser writing, Appl. Phys. 123 (2017) 698, https://doi.org/10.1007/s00339-017-1303-9.

[32] D.S. Simon, Bessel beams, self-healing and diffraction free propagation, in: A Guided Tour of Light beams, Morgan and Claypool publishers, California, 2016.

[33] B. Caylar, M. Pomorski, P. Bergonzo, Laser-processed three dimensional graphitic electrodes for diamond radiation detectors, Appl. Phys. Lett. 103 (2013), 043504, https://doi.org/10.1063/1.4816328.

[34] V.N. Strekalov, V.I. Konov, V.V. Kononenko, S.M. Pimenov, Early stages of laser graphitization of diamond, Appl. Phys. 76 (2003) 603–607, https://doi.org/10.1007/s00339-002-2014-3.

[35] B. Sotillo, A. Chiappini, V. Bharadwaj, J.P. Hadden, F. Bosia, P. Olivero, M. Ferrari, R. Ramponi, P.E. Barclay, S.M. Eaton, Polarized micro-Raman studies of femtosecond laser written stress-induced optical waveguides in diamond, Appl. Phys. Lett. 112 (2018), 031109, https://doi.org/10.1063/1.5017108.

[36] R.H. Telling, C.J. Pickard, M.C. Payne, J.E. Field, Theoretical strength and cleavage of diamond, Phys. Rev. Lett. 84 (2000) 5160–5163, https://doi.org/10.1103/PhysRevLett.84.5160.

[37] I. Haughton, I. Lopez Paz, M. McGowan, A. Oh, A. Porter, P.S. Salter, O. Allegre, Barrier potential for laser written graphitic wires in diamond, Diam. Relat. Mater. 111 (2021), 108164, https://doi.org/10.1016/j.diamond.2020.108164.

[38] S. Lagomarsino, M. Bellini, C. Corsi, S. Fanetti, F. Gorelli, I. Liontos, G. Parrini, M. Santoro, S. Sciortino, Electrical and Raman-imaging characterization of laser-made electrodes for 3D diamond detectors, Diam. Relat. Mater. 43 (2014) 23–28, https://doi.org/10.1016/j.diamond.2014.01.002.

[39] P.S. Salter, M.J. Booth, A. Courvoisier, D.A.J. Moran, D.A. MacLaren, High resolution structural characterisation of laser-induced defect clusters inside diamond, Appl. Phys. Lett. 111 (2017), 081103, https://doi.org/10.1063/1.4993118.

[40] K.K. Ashikkalieva, T.V. Kononenko, E.A. Obraztsova, E.V. Zavedeev, A.A. Khomich, E.E. Ashkinazi, V.I. Konov, Direct observation of graphenic nanostructures inside femtosecond-laser modified diamond, Carbon 102 (2016) 383–389, https://doi.org/10.1016/j.carbon.2016.02.044.

[41] J. Sánchez-González, A. Macías-García, M.F. Alexandre-Franco, V. Gómez-Serrano, Electrical conductivity of carbon blacks under compression, Carbon 43 (2005) 741–747, https://doi.org/10.1016/j.carbon.2004.10.045.

[42] A. Oh, B. Caylar, M. Pomorski, T. Wengler, A novel detector with graphitic electrodes in CVD diamond, Diam. Relat. Mater. 38 (2013) 9–13, https://doi.org/10.1016/j.diamond.2013.06.003.

[43] M. Shimizu, Y. Shimotsuma, M. Sakakura, T. Yuasa, H. Homma, Y. Minowa, K. Tanaka, K. Miura, K. Hirao, Periodic metallo-dielectric structure in diamond, Opt. Express 17 (2009) 46–54, https://doi.org/10.1364/OE.17.000046.